Charged Higgs production in association with a top quark at approximate NNLO

Nikolaos Kidonakis

Department of Physics, Kennesaw State University, Kennesaw, Georgia 30144, USA

I present approximate next-to-next-to-leading-order (aNNLO) total and differential cross sections for charged Higgs production in association with a top quark at LHC energies. The aNNLO results for the process $bg \rightarrow tH^-$ are derived from next-to-next-to-leading-logarithm (NNLL) resummation of soft-gluon corrections. Scale and parton-distribution uncertainties for the cross sections are shown. The top-quark transverse-momentum and rapidity distributions are also calculated.

I. INTRODUCTION

The Higgs sector of the standard model and its extensions is a focus of particle physics theoretical and experimental programs. In two-Higgs-doublet models, such as the minimal supersymmetric standard model, one Higgs doublet gives mass to the up-type fermions while the other to the down-type fermions. The ratio of the vacuum expectation values for the two doublets is denoted by $\tan \beta$. Among the five Higgs particles in such models there are two charged Higgs bosons, H^+ and H^-.

QCD and SUSY-QCD corrections for the associated production of a charged Higgs boson and a top quark via the partonic process $bg \rightarrow tH^-$ have been calculated through next-to-leading order (NLO) in Refs. [1–9]. The NLO corrections provide a substantial enhancement of the cross section and they reduce the scale dependence.

An important class of radiative corrections comes from soft-gluon emission. Near partonic threshold for the production of the tH^- final state these soft-gluon logarithmic corrections are dominant and large; thus, their inclusion is necessary to extend the precision of the theoretical predictions beyond NLO.

Higher-order soft-gluon corrections for tH^- production were calculated in Refs. [10–15]. It was shown in Ref. [11] that at NLO the soft-gluon corrections approximate very well the exact NLO result, the difference being of the order of only a few percent. This proves the importance and numerical dominance of the soft-gluon corrections and is in agreement with similar observations for other top-quark processes (see e.g. [14,15]). Thus, we expect that at next-to-next-to-leading order (NNLO) the soft-gluon corrections will also approximate future exact results very well (this expectation has been validated for related top production processes [15]).

The approximate NNLO (aNNLO) corrections were first derived from next-to-leading-logarithm (NLL) resummation in [10,11] and later improved with next-to-next-to-leading-logarithm (NNLL) resummation in [14]. The aNNLO corrections are significant and they further enhance the cross section.

There have been ongoing active searches for charged Higgs bosons, first at the Tevatron [16,17] and more recently at the LHC [18,19]. The increase in the expected theoretical cross section should be taken into account in these searches and in the setting of limits for charged Higgs production in association with a top quark.

In the next section we provide some theoretical discussion and results for the soft-gluon corrections in tH^- production. In Sec. III we present total cross sections for tH^- production at LHC energies, with various choices of charged Higgs mass as well as $\tan \beta$, noting that the cross sections for $\bar{t}H^+$ production are the same. In Sec. IV we present the top-quark transverse-momentum and rapidity distributions in this process. We conclude in Sec. V.

II. SOFT-GLUON CORRECTIONS FOR tH^- PRODUCTION

We study tH^- production in collisions of protons A and B. The leading-order (LO) diagrams for $bg \rightarrow tH^-$ are shown in Fig. 1. The hadronic kinematical variables for the process $A(p_A) + B(p_B) \rightarrow t(p_t) + H^-(p_{H^-})$ are $S = (p_A + p_B)^2$, $T = (p_A - p_t)^2$, and $U = (p_B - p_t)^2$. For the partonic reaction $b(p_b) + g(p_g) \rightarrow t(p_t) + H^-(p_{H^-})$, the partonic kinematical variables are $s = (p_b + p_g)^2$, $t = (p_b - p_t)^2$, and $u = (p_g - p_t)^2$, with $p_b = x_1 p_A$ and $p_g = x_2 p_B$. We also define the threshold variable $s_4 = s + t + u - m_t^2 - m_{H^-}^2$, where m_{H^-} is the charged Higgs mass and m_t is the top quark mass. Note that s_4
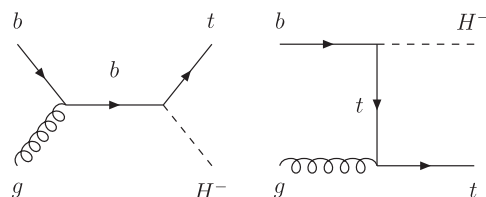

FIG. 1. Leading-order diagrams for $bg \rightarrow tH^-$.

014010-1

measures any additional radiation and it vanishes at partonic threshold.

The double-differential LO cross section is $d^2\hat{\sigma}_{\text{LO}}^{bg\to tH^-}/(dt du) = F_{\text{LO}}^{bg\to tH^-}\delta(s_4)$ where

$$F_{\text{LO}}^{bg\to tH^-} = \frac{\pi\alpha\alpha_s(m_b^2\tan^2\beta + m_t^2\cot^2\beta)}{12s^2 m_W^2\sin^2\theta_w}\left\{\frac{s+t-m_{H^-}^2}{2s}\right.$$
$$- \frac{m_t^2(u-m_{H^-}) + m_{H^-}^2(t-m_t^2) + s(u-m_t^2)}{s(u-m_t^2)}$$
$$\left. - \frac{m_t^2(u-m_{H^-}^2 - s/2) + su/2}{(u-m_t^2)^2}\right\}, \quad (2.1)$$

where $\alpha = e^2/(4\pi)$, α_s is the strong coupling, θ_w is the weak-mixing angle, m_W is the W boson mass, and m_b is the b-quark mass which is taken to be zero everywhere except in the $m_b^2\tan^2\beta$ term.

The perturbative nth-order soft-gluon corrections appear as logarithmic plus-distribution enhancements, $[\ln^k(s_4/m_{H^-}^2)/s_4]_+$, with $0 \leq k \leq 2n-1$. These corrections can be derived from resummation, starting with the factorization properties of the cross section in moment space. We write moments of the partonic cross section $\hat{\sigma}(N) = \int(ds_4/s)e^{-Ns_4/s}\hat{\sigma}(s_4)$, with N the moment variable. Logarithms of s_4 in the physical cross section give rise to logarithms of N in moment space, and those logarithms of N exponentiate.

The factorized expression for the moment-space partonic cross section in $n = 4 - \epsilon$ dimensions is

$$\hat{\sigma}^{bg\to tH^-}(N,\epsilon) = H^{bg\to tH^-}(\alpha_s(\mu))S^{bg\to tH^-}\left(\frac{m_{H^-}}{N\mu}, \alpha_s(\mu)\right)$$
$$(2.2)$$

with μ the scale. Here the hard function $H^{bg\to tH^-}$ involves contributions from the amplitude of the process and its complex conjugate, while $S^{bg\to tH^-}$ is the soft function for noncollinear soft-gluon emission and it represents the coupling of soft gluons to the partons in the scattering.

The product of the hard and soft functions in Eq. (2.2) is independent of the gauge and the factorization scale, and its evolution results in the exponentiation of logarithms of N. The soft function $S^{bg\to tH^-}$ requires renormalization and thus its N-dependence can be resummed via renormalization group evolution. We have

$$S_{\text{bare}}^{bg\to tH^-} = Z_S^{\dagger bg\to tH^-}S^{bg\to tH^-}Z_S^{bg\to tH^-} \quad (2.3)$$

where $S_{\text{bare}}^{bg\to tH^-}$ is the unrenormalized function, and $Z_S^{bg\to tH^-}$ is a renormalization constant.

Thus, $S^{bg\to tH^-}$ satisfies the renormalization-group equation

$$\left(\mu\frac{\partial}{\partial\mu} + \beta(g_s,\epsilon)\frac{\partial}{\partial g_s}\right)S^{bg\to tH^-} = -2S^{bg\to tH^-}\Gamma_S^{bg\to tH^-}.$$
$$(2.4)$$

In the above equation $g_s^2 = 4\pi\alpha_s$; $\beta(g_s,\epsilon) = -g_s\epsilon/2 + \beta(g_s)$ where $\beta(g_s)$ is the QCD beta function $\beta(g_s) \equiv \mu dg_s/d\mu$; and $\Gamma_S^{bg\to tH^-}$ is the soft anomalous dimension that controls the evolution of the soft function $S^{bg\to tH^-}$:

$$\Gamma_S^{bg\to tH^-} = \frac{dZ_S^{bg\to tH^-}}{d\ln\mu}(Z^{-1})_S^{bg\to tH^-}. \quad (2.5)$$

Writing $\Gamma_S^{bg\to tH^-} = (\alpha_s/\pi)\Gamma_S^{(1)} + (\alpha_s/\pi)^2\Gamma_S^{(2)} + \cdots$, we have [14]

$$\Gamma_S^{(1)} = C_F\left[\ln\left(\frac{m_t^2 - t}{m_t\sqrt{s}}\right) - \frac{1}{2}\right] + \frac{C_A}{2}\ln\left(\frac{m_t^2 - u}{m_t^2 - t}\right) \quad (2.6)$$

and

$$\Gamma_S^{(2)} = \left[C_A\left(\frac{67}{36} - \frac{\zeta_2}{2}\right) - \frac{5}{18}n_f\right]\Gamma_S^{(1)} + C_F C_A\frac{(1-\zeta_3)}{4}$$
$$(2.7)$$

where $C_F = (N_c^2 - 1)/(2N_c)$ and $C_A = N_c$, with $N_c = 3$ the number of colors, and $n_f = 5$ is the number of light-quark flavors.

The resummed cross section in moment space is derived from the renormalization-group evolution of the hard and soft functions in the factorized cross section, Eq. (2.2), and is given by:

$$\hat{\sigma}_{\text{resummed}}^{bg\to tH^-}(N) = \exp\left[\sum_{i=b,g}E_i(N_i)\right]H^{bg\to tH^-}(\alpha_s(\sqrt{s}))$$
$$\times S^{bg\to tH^-}\left(\alpha_s\left(\frac{\sqrt{s}}{N'}\right)\right)$$
$$\times \exp\left[\int_{\sqrt{s}}^{\sqrt{s}/N'}\frac{d\mu}{\mu}2\Gamma_S^{bg\to tH^-}(\alpha_s(\mu))\right] \quad (2.8)$$

where the first exponent resums soft and collinear radiation from the incoming bottom quark and gluon, and the second exponent resums noncollinear soft-gluon emission (see [14] for more details).

The resummed cross section in moment space can be expanded in powers of the strong coupling and inverted back to momentum space, thus providing approximate results for the higher-order corrections from soft-gluon emission. The aNNLO soft-gluon corrections in the double-differential partonic cross section, $d^2\hat{\sigma}/(dt du)$, can be written as

$$\frac{d^2\hat{\sigma}_{\text{aNNLO}}^{(2)bg\to tH^-}}{dtdu} = F_{\text{LO}}^{bg\to tH^-}\frac{\alpha_s^2}{\pi^2}\sum_{k=0}^{3}C_k^{(2)}\left[\frac{\ln^k(s_4/m_{H^-}^2)}{s_4}\right]_+ \quad (2.9)$$

where the superscript "(2)" in $\hat{\sigma}$ and $C_k^{(2)}$ indicates that these are second-order corrections in the strong coupling. The leading aNNLO coefficient, $C_3^{(2)}$, depends only on color factors: $C_3^{(2)} = 2(C_F + C_A)^2$.

The subleading coefficients $C_2^{(2)}$, $C_1^{(2)}$, and $C_0^{(2)}$ are in general functions of s, t, u, m_{H^-}, m_t, and the factorization scale μ_F, and—in the case of $C_1^{(2)}$ and $C_0^{(2)}$—also the renormalization scale μ_R. These coefficients have been determined from one-loop [10,11] and two-loop [14] calculations. The next-to-leading coefficient is

$$C_2^{(2)} = (C_F + C_A)\left\{3C_F\left[2\ln\left(\frac{m_t^2 - t}{m_t\sqrt{s}}\right) - 2\ln\left(\frac{m_{H^-}^2 - u}{m_{H^-}^2}\right) - 1\right]\right.$$
$$- 3C_A\left[\ln\left(\frac{m_t^2 - t}{m_t^2 - u}\right) + 2\ln\left(\frac{m_{H^-}^2 - t}{m_{H^-}^2}\right)\right]$$
$$\left. - 3(C_F + C_A)\ln\left(\frac{\mu_F^2}{s}\right) - \frac{\beta_0}{2}\right\} \quad (2.10)$$

where $\beta_0 = (11C_A - 2n_f)/3$. The expressions for $C_1^{(2)}$ and $C_0^{(2)}$ are much longer [14]. With NLL resummation [10,11] we can calculate all aNNLO coefficients except $C_0^{(2)}$, which can only be fully determined by NNLL resummation [14]. The one-loop soft anomalous dimension, $\Gamma_S^{(1)}$, contributes to all subleading coefficients, while the two-loop soft anomalous dimension, $\Gamma_S^{(2)}$, contributes to $C_0^{(2)}$.

The hadronic differential cross section can be calculated via a convolution of the partonic cross section with parton distribution functions (pdf). The double-differential cross section with respect to the top-quark transverse momentum, p_T, and rapidity, Y, is given by

$$\frac{d\sigma}{dp_T dY} = 2p_T\int_{x_{2\min}}^{1}dx_2\int_0^{s_{4\max}}ds_4\frac{x_1 x_2 S}{x_2 S + T_1}\phi(x_1)\phi(x_2)$$
$$\times\frac{d^2\hat{\sigma}^{bg\to tH^-}}{dtdu} \quad (2.11)$$

where $T_1 = T - m_t^2 = -\sqrt{S}(m_t^2 + p_T^2)^{1/2}e^{-Y}$, $U_1 = U - m_t^2 = -\sqrt{S}(m_t^2 + p_T^2)^{1/2}e^Y$, $x_{2\min} = (m_{H^-}^2 - T)/(S + U_1)$, $s_{4\max} = x_2(S + U_1) + T - m_{H^-}^2$, $x_1 = (s_4 - m_t^2 + m_{H^-}^2 - x_2 U_1)/(x_2 S + T_1)$; and ϕ denotes the pdf. The transverse-momentum and rapidity distributions as well as the total cross section can be obtained by appropriate integrations over this double-differential cross section.

III. tH^- TOTAL CROSS SECTIONS

We continue with results for the total cross sections for charged Higgs production in association with a top quark via the partonic process $bg \to tH^-$ at LHC energies. The results we present are for tH^- production; the cross sections for $\bar{t}H^+$ production are identical. We use the MMHT2014 [20] NNLO pdf for all our numerical results in this paper.

In Fig. 2 we plot the total cross sections at aNNLO for tH^- production as functions of charged Higgs mass at 7, 8, 13, and 14 TeV energies at the LHC. The left plot shows the results with $\tan\beta = 10$ while the right plot shows the corresponding results with $\tan\beta = 30$. The scales are set equal to the charged Higgs mass. Since the $\tan\beta$ dependence is simply given by the $(m_b^2\tan^2\beta + m_t^2\cot^2\beta)$ factor in Eq. (2.1), one can easily rescale the results to any desired $\tan\beta$ value. We note that the cross sections decrease over three orders of magnitude as the charged Higgs mass is increased from 200 GeV to 1500 GeV.
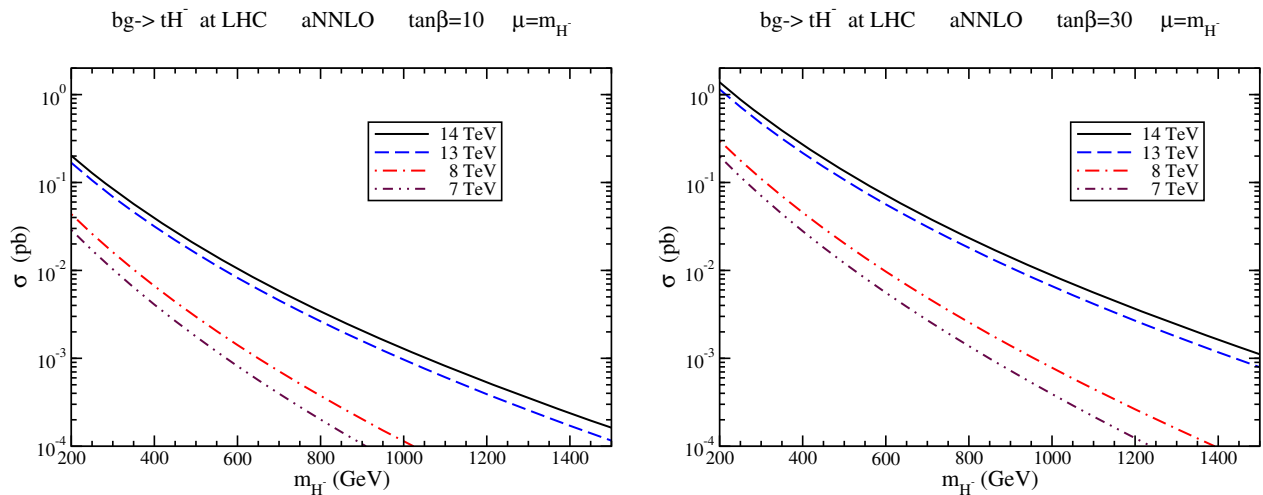

FIG. 2.   Total aNNLO cross sections for tH^- production at 7, 8, 13, and 14 TeV LHC energy with (left) $\tan\beta = 10$ and (right) $\tan\beta = 30$.

TABLE I. The aNNLO tH^- production cross section in fb in pp collisions at the LHC with $\sqrt{S} = 7$, 8, 13, and 14 TeV. We set $\tan\beta = 30$ and $\mu = m_{H^-}$, and we use the MMHT2014 NNLO pdf [20].

aNNLO tH^- cross section with $\tan\beta = 30$ at LHC (fb)				
m_{H^-} (GeV)	7 TeV	8 TeV	13 TeV	14 TeV
200	198	299	1148	1382
400	28.0	45.5	217	269
600	5.58	9.70	56.4	71.7
800	1.38	2.57	18.1	23.5
1000	0.393	0.782	6.62	8.81

In Table I we provide some numbers for the total cross sections for selected values of charged Higgs mass at LHC energies of 7, 8, 13, and 14 TeV. The values are for $\tan\beta = 30$ and scale $\mu = m_{H^-}$.

In Fig. 3 we plot the aNNLO/NLO ratios, i.e. K factors, for the total cross sections for tH^- production as functions of charged Higgs mass. The $\tan\beta$ dependence of course cancels out in K factors. The left plot displays results at 13 TeV LHC energy. The line labeled as "central" is with the scales set equal to the charged Higgs mass. The lines labeled as "scale" show the variation when the scales in the aNNLO cross section are varied by a factor of two (but the NLO denominator is always kept at scale $\mu = m_{H^-}$). The lines labeled as "scale + pdf" show the total uncertainty including scale variation plus uncertainties from the NNLO parton distribution functions as given by [20]. We see that the K factors are sizable, indicating significant contributions of 15% to 20%—depending on the charged Higgs mass—from the central aNNLO corrections. The right plot shows the central K factors at 7, 8, 13, and 14 TeV LHC energies. The K factors are larger at the
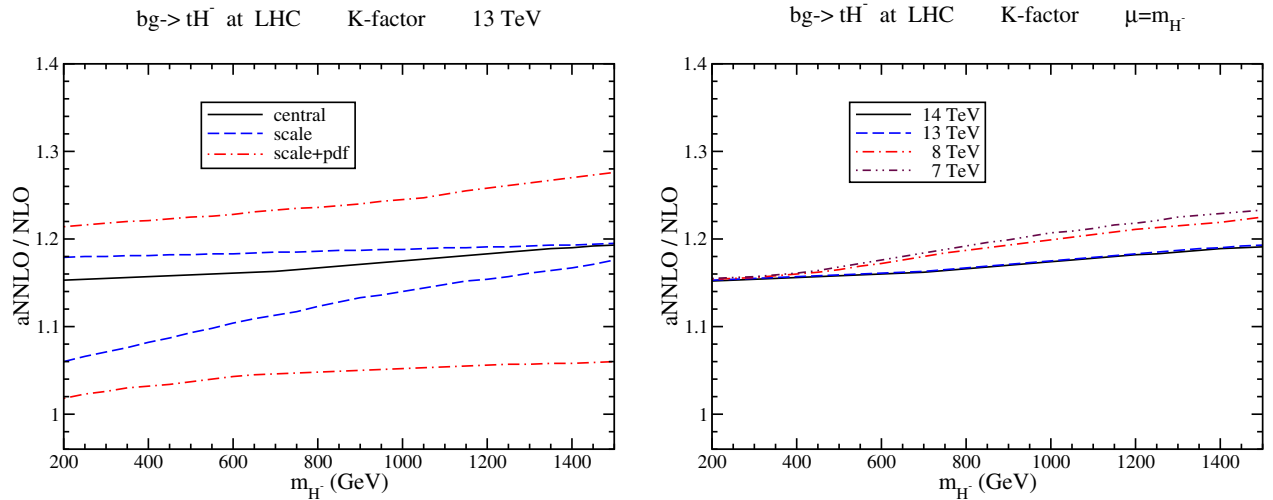

FIG. 3. aNNLO/NLO K-factors for the total cross section for tH^- production at (left) 13 TeV LHC energy and (right) 7, 8, 13, and 14 TeV LHC energies.
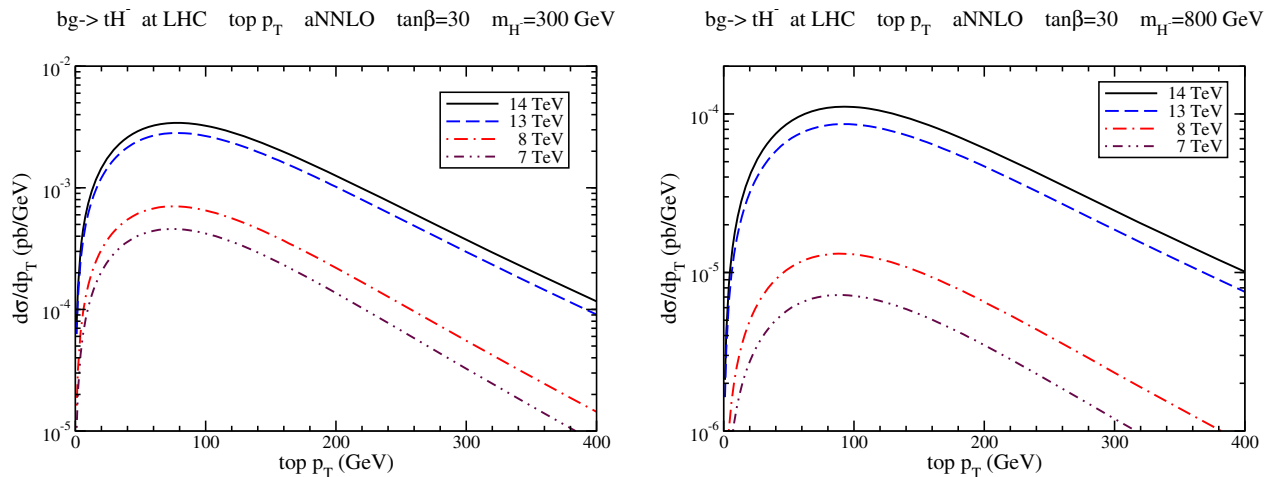

FIG. 4. aNNLO top-quark p_T distributions, $d\sigma/dp_T$, in tH^- production with $\tan\beta = 30$ at 7, 8, 13, and 14 TeV LHC energy with (left) $m_{H^-} = 300$ GeV and (right) $m_{H^-} = 800$ GeV.
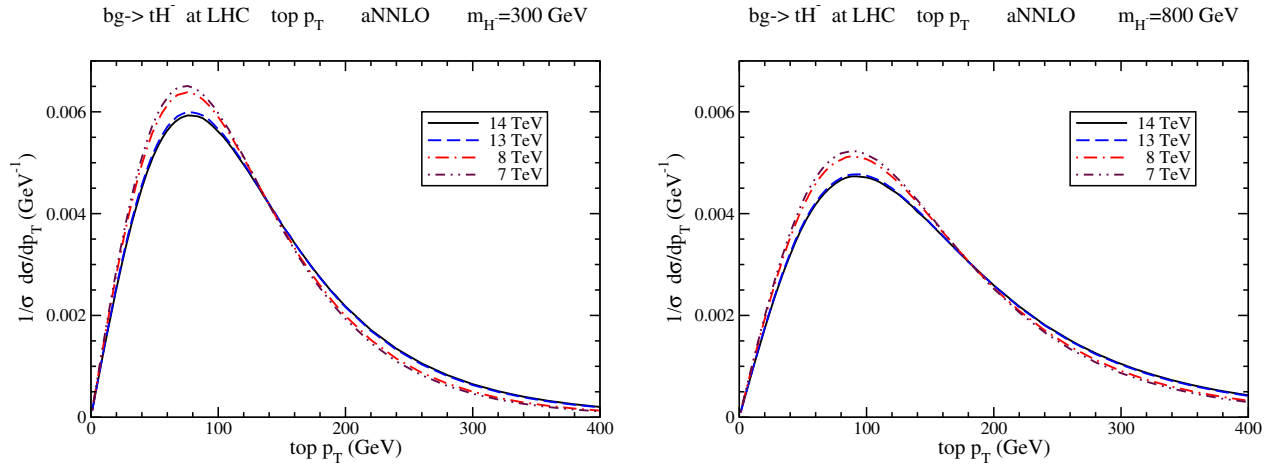
FIG. 5.   aNNLO top-quark normalized p_T distributions, $(1/\sigma)d\sigma/dp_T$, in tH^- production at 7, 8, 13, and 14 TeV LHC energy with (left) $m_{H^-} = 300$ GeV and (right) $m_{H^-} = 800$ GeV.

smaller LHC energies, since then the process is closer to partonic threshold.

We note that scale variation is supposed to give an indication of theoretical uncertainty due to higher-order missing terms. Of course for an approximate calculation there is also uncertainty due to the approximation; however, there is no independent way to calculate that. The comparison to fixed-order results when those are available can indicate the effectiveness of the approximation both for the central scale choice and for the scale variation. Since at NLO the soft-gluon approximation works very well for tH^- production, this would indicate that the scale variation at aNNLO is an adequate representation of the theoretical uncertainty. Again, this has been shown to be a valid assumption from related studies of top-antitop production [15]. At NLO both the central result and the scale variation were very similar between exact and approximate results for that process, and the expectation was that this would also hold at NNLO. This expectation was indeed valid as proven later by the

comparison of central results and scale variation between exact NNLO and aNNLO predictions as discussed in [15].

IV. TOP-QUARK p_T AND RAPIDITY DISTRIBUTIONS

We continue with a presentation of differential distributions in tH^- production, in particular the top-quark transverse-momentum and rapidity distributions.

In Fig. 4 we plot the top-quark transverse-momentum distributions, $d\sigma/dp_T$, at aNNLO with $\tan\beta = 30$ for 7, 8, 13, and 14 TeV LHC energies. The left plot uses $m_{H^-} = 300$ GeV and the right plot uses $m_{H^-} = 800$ GeV. One can derive results for any value of $\tan\beta$ with appropriate rescaling. For $m_{H^-} = 300$ GeV the distributions peak at p_T values of around 75 GeV and drop by two orders of magnitude at a p_T of 400 GeV. For $m_{H^-} = 800$ GeV the distributions are much smaller due to the very heavy final state.
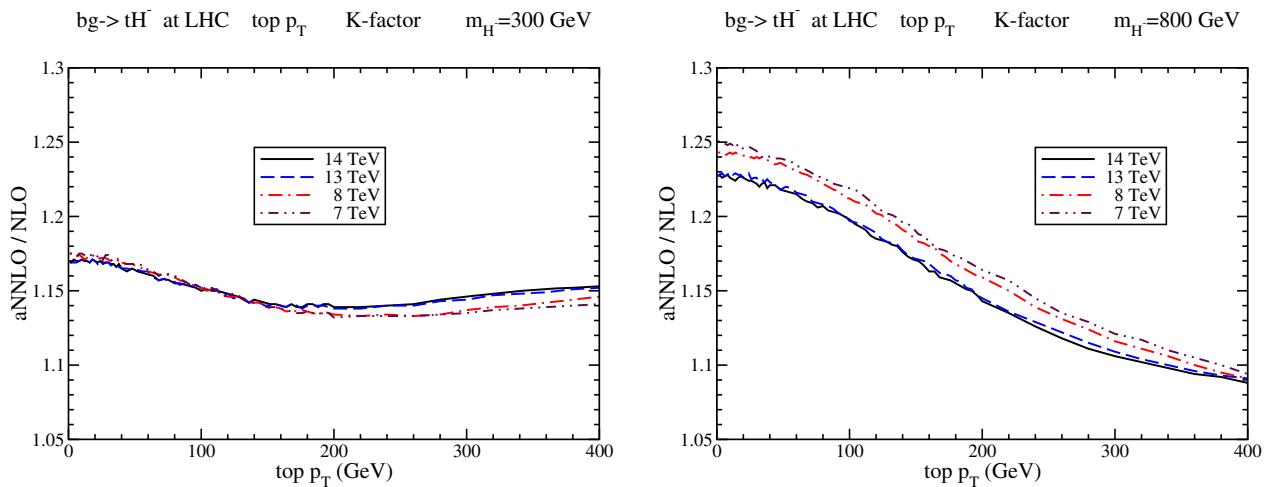

FIG. 6.   The aNNLO/NLO K-factors for the top-quark p_T distributions, $d\sigma/dp_T$, in tH^- production at 7, 8, 13, and 14 TeV LHC energy with (left) $m_{H^-} = 300$ GeV and (right) $m_{H^-} = 800$ GeV.

bg->tH⁻ at LHC   top rapidity   aNNLO   tanβ=30   m_H=300 GeV

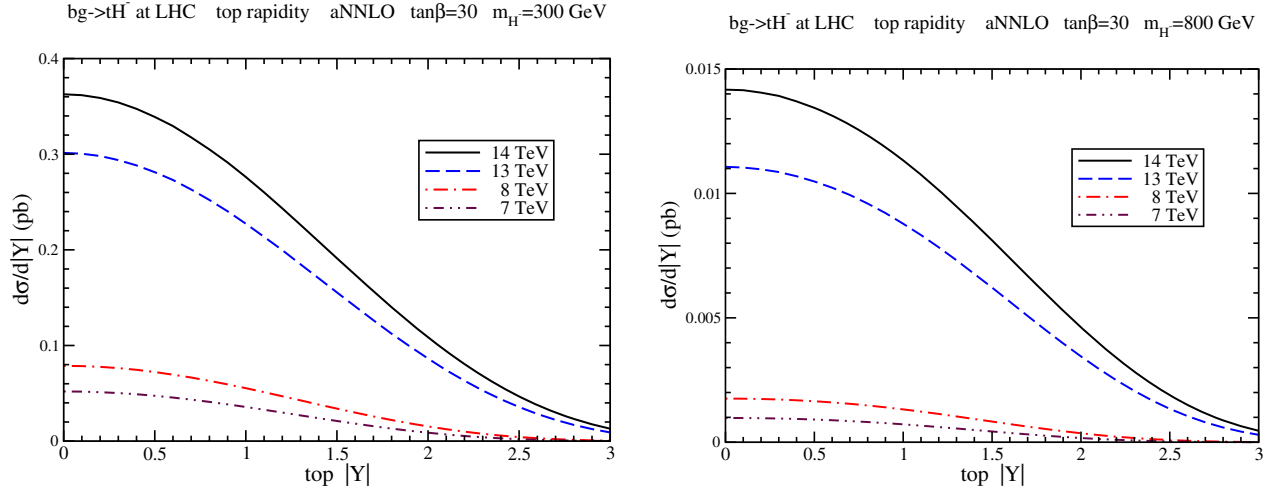bg->tH⁻ at LHC   top rapidity   aNNLO   tanβ=30   m_H=800 GeV

FIG. 7.   aNNLO top-quark rapidity distributions, $d\sigma/d|Y|$, in tH^- production with $\tan\beta = 30$ at 7, 8, 13, and 14 TeV LHC energy with (left) $m_{H^-} = 300$ GeV and (right) $m_{H^-} = 800$ GeV.

bg->tH⁻ at LHC   top rapidity   aNNLO   m_H=300 GeV

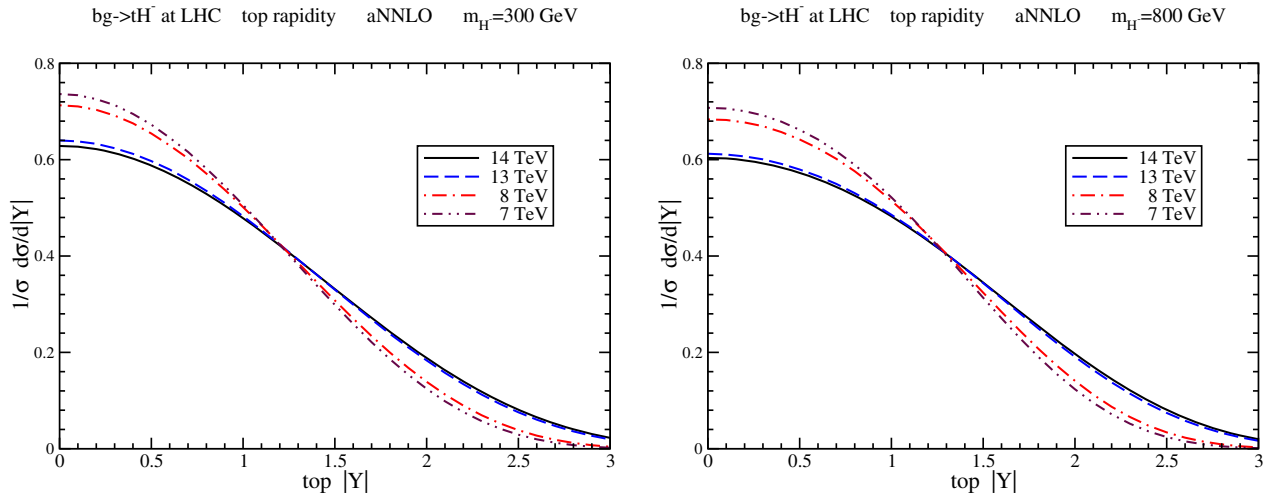bg->tH⁻ at LHC   top rapidity   aNNLO   m_H=800 GeV

FIG. 8.   aNNLO top-quark normalized rapidity distributions, $(1/\sigma)d\sigma/d|Y|$, in tH^- production at 7, 8, 13, and 14 TeV LHC energy with (left) $m_{H^-} = 300$ GeV and (right) $m_{H^-} = 800$ GeV.

In Fig. 5 we plot the normalized top-quark transverse-momentum distributions, $(1/\sigma)d\sigma/dp_T$, at aNNLO for LHC energies. The left plot is with $m_{H^-} = 300$ GeV and the right plot is with $m_{H^-} = 800$ GeV. The use of normalized distributions removes the $\tan\beta$ dependence and minimizes the dependence on the pdf. The dependence on the charged Higgs mass is also milder for the normalized distributions. We note that at lower LHC energies the normalized top p_T distribution is somewhat smaller at large p_T than it is at higher energies, as expected.

Figure 6 shows the aNNLO/NLO ratios, i.e. K factors, for the top-quark transverse-momentum distributions at LHC energies. The left plot has $m_{H^-} = 300$ GeV and the right plot has $m_{H^-} = 800$ GeV. The aNNLO contributions are clearly seen to be quite significant, around 15% for most p_T values when $m_{H^-} = 300$ GeV. Again, the $\tan\beta$ dependence cancels out in the K factors.

In Fig. 7 we plot the top-quark rapidity distributions, $d\sigma/d|Y|$, at aNNLO with $\tan\beta = 30$ for 7, 8, 13, and 14 TeV LHC energies. The left plot uses $m_{H^-} = 300$ GeV and the right plot uses $m_{H^-} = 800$ GeV. The distributions at 800 GeV mass are of course much smaller. As before, one can derive results for any value of $\tan\beta$ with appropriate rescaling.

In Fig. 8 we plot the normalized top-quark rapidity distributions, $(1/\sigma)d\sigma/d|Y|$, at aNNLO for LHC energies. The left plot is with $m_{H^-} = 300$ GeV and the right plot is with $m_{H^-} = 800$ GeV. We note that at lower energies the normalized top rapidity distribution is smaller at large absolute values of $|Y|$ than it is at higher energies, as expected.

Figure 9 shows the aNNLO/NLO ratios, i.e. K factors, for the top-quark rapidity distributions at LHC energies. The left plot has $m_{H^-} = 300$ GeV and the right plot has $m_{H^-} = 800$ GeV. The aNNLO contributions are quite significant, especially at large rapidity. At 7 TeV LHC energy
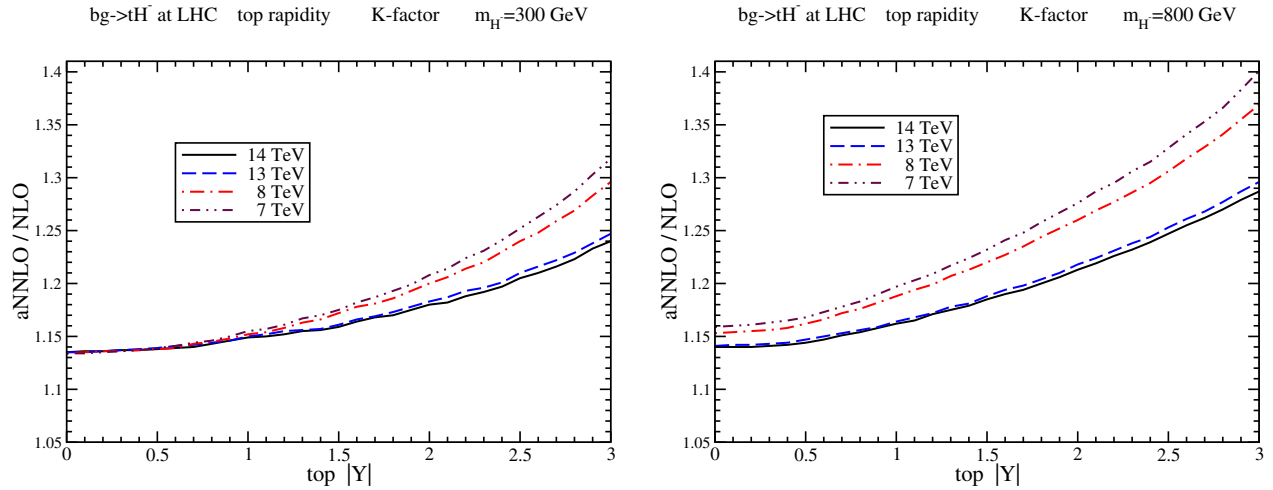
bg->tH⁻ at LHC   top rapidity   K-factor m_H=300 GeV   bg->tH⁻ at LHC   top rapidity   K-factor m_H=800 GeV

FIG. 9.   The aNNLO/NLO K-factors for the top-quark rapidity distributions, $d\sigma/d|Y|$, in tH^- production at 7, 8, 13, and 14 TeV LHC energy with (left) $m_{H^-} = 300$ GeV and (right) $m_{H^-} = 800$ GeV.

and 800 GeV mass, the aNNLO corrections are 40% at $|Y| = 3$.

V. CONCLUSIONS

I have presented aNNLO results for charged Higgs production in association with a top quark via the partonic process $bg \to tH^-$. Total cross sections and top-quark p_T and rapidity distributions have been calculated at LHC energies. The NNLO soft-gluon contributions are important and provide significant enhancements of the total cross sections. Uncertainties due to scale variations and due to the parton distribution functions have also been presented.

The top-quark differential distributions in transverse momentum and rapidity also receive significant enhancements from soft-gluon contributions. The corrections are particularly large at large rapidity values.

The aNNLO corrections need to be included in theoretical predictions for total cross sections and differential distributions in order to provide more precision in the search for charged Higgs bosons.

[1] A. Belyaev, D. Garcia, J. Guasch, and J. Sola, Phys. Rev. D **65**, 031701 (2002); J. High Energy Phys. 06 (2002) 059.
[2] S.-H. Zhu, Phys. Rev. D **67**, 075006 (2003).
[3] G.-P. Gao, G.-R. Lu, Z.-H. Xiong, and J. M. Yang, Phys. Rev. D **66**, 015007 (2002).
[4] T. Plehn, Phys. Rev. D **67**, 014018 (2003).
[5] E. L. Berger, T. Han, J. Jiang, and T. Plehn, Phys. Rev. D **71**, 115012 (2005).
[6] W. Peng, M. Wen-Gan, Z. Ren-You, J. Yi, H. Liang, and G. Lei, Phys. Rev. D **73**, 015012 (2006); **80**, 059901(E) (2009).
[7] S. Dittmaier, M. Kramer, M. Spira, and M. Walser, Phys. Rev. D **83**, 055005 (2011).
[8] M. Flechl, R. Klees, M. Kramer, M. Spira, and M. Ubiali, Phys. Rev. D **91**, 075015 (2015).
[9] C. Degrande, M. Ubiali, M. Wiesemann, and M. Zaro, J. High Energy Phys. 10 (2015) 145.
[10] N. Kidonakis, Int. J. Mod. Phys. A **19**, 1793 (2004); Mod. Phys. Lett. A **19**, 405 (2004).

[11] N. Kidonakis, J. High Energy Phys. 05 (2005) 011.
[12] N. Kidonakis, Phys. Rev. D **73**, 034001 (2006).
[13] N. Kidonakis, Proc. Sci. HEP2005 (2005) 336 [arXiv: hep-ph/0511235]; CHARGED2008 (2008) 003 [arXiv: 0811.4757].
[14] N. Kidonakis, Phys. Rev. D **82**, 054018 (2010).
[15] N. Kidonakis, arXiv:1311.0283.
[16] V. M. Abazov et al. (D0 Collaboration), Phys. Rev. D **80**, 051107 (2009); Phys. Lett. B **682**, 278 (2009).
[17] T. Aaltonen et al. (CDF Collaboration), Phys. Rev. Lett. **103**, 101803 (2009).
[18] G. Aad et al. (ATLAS Collaboration), J. High Energy Phys. 06 (2012) 039; 03 (2013) 076; 03 (2015) 088; 03 (2016) 127; Phys. Lett. B **759**, 555 (2016).
[19] S. Chatrchyan et al. (CMS Collaboration), J. High Energy Phys. 07 (2012) 143; 11 (2015) 018; 12 (2015) 178.
[20] L. A. Harland-Lang, A. D. Martin, P. Molytinski, and R. S. Thorne, Eur. Phys. J. C **75**, 204 (2015).